Optics & Laser Technology 144 (2021) 107393

Contents lists available at ScienceDirect

Optics and Laser Technology

journal homepage: www.elsevier.com/locate/optlastec

A Raman study on nanosecond-laser-induced multi-level switching of $Ge_2Sb_2Te_5$ thin films

Jia Du [a], Zhangjian Mu [a], Lan Li [b,c], Junying Li [d,*]

[a] Shanghai Key Laboratory of Modern Optical System, School of Optical-Electrical and Computer Engineering, University of Shanghai for Science and Technology, Shanghai 200093, China
[b] Key Laboratory of 3D Micro/Nano Fabrication and Characterization of Zhejiang Province, School of Engineering, Westlake University, Hangzhou 310024, China
[c] Institute of Advanced Technology, Westlake Institute for Advanced Study, Hangzhou 310024, China
[d] College of Information Science and Electronic Engineering, Zhejiang University, Hangzhou 310027, China

ARTICLE INFO

Keywords:
Phase change material
Laser-induced phase transition
Multi-level switching
Raman spectroscopy

ABSTRACT

As one of the most successful nonvolatile phase change materials (PCMs), $Ge_2Sb_2Te_5$ (GST) can be reversibly switched between amorphous and crystalline phases by nanosecond laser pulses, which enables its applications in optical disks and various emerging reconfigurable photonic devices. Instead of simply inducing temperature rising of GST thin film via light absorption, high-energy laser irradiation leads to modifications of molecular bonds, forming different local structures. We employed a nanosecond pulse laser with different pulse duration, energy and pulse numbers to induce multi-level switching of GST thin films. By employing Raman spectroscopy, we illustrated that $GeTe_{4-n}Ge_n$ (n = 0, 1, 2) subsystem plays a decisive role in laser-induced crystallization of GST. Different from isothermal annealing, where Sb_mTe_3 (m = 1, 2) subsystem contributes as well. This is evidenced by the suppression of Sb_mTe_3 structure of an isothermally annealed film treated with additional laser crystallization. In addition, our investigations indicated that in $GeTe_{4-n}Ge_n$ subsystem, Joule heating promotes the formation of Te-rich tetrahedral components. These findings provide more insights into the structural characteristics of GST.

1. Introduction

Chalcogenide-based PCMs, a unique group of materials featuring rapid and reversible phase switching as well as the large contrast in electrical and optical properties between amorphous and crystalline states, have found widespread adoption in data storage [1–5], photonic switches and routers [6,7], reconfigurable meta-optics [4,8], electrically- or optically- driven intelligent displays [4,9], sensors [10], and optical neuromorphic computers [2,5], etc. Among numerous phase change materials, $Ge_1Sb_2Te_4$, $Ge_2Sb_2Te_5$ (GST), $Ge_1Sb_4Te_7$, $Ge_8Sb_2Te_{11}$ and other pseudo binary alloys on GeTe-Sb_2Te_3 tie-line were widely studied and employed [5,11–13]. Particularly, the typical GST material successfully combines the merits of fast phase switching speed, large contrast and high thermal stability [3,5]. The phase transition of GST can be triggered by thermal annealing, laser irradiation and electrical pulses, among which the last two allow reversible phase changes between amorphous and crystalline states. The reversible phase switching is very important to PCMs-based devices, as this allows reconfigurable operation of the device functionality. During the reversible phase switching process, a high-power short electrical or laser pulse can lead to melt-and-quench amorphization in phase change material, while a relatively lower-power and longer pulse (or a pulse train) can result in crystallization.

Laser-induced switching is of great interest to photonic and optical devices due to the simplified device structure and its significant role in all-optical photonic circuits and flat optical components. The amorphization process of GST typically occurs in tens of nanoseconds, while crystallization process is extended to tens to hundreds of nanoseconds, due to the minimum time required for the nuclei to form and grow [14,15]. Considerable amount of works have been focused on the study of the amorphization and crystallization behavior of laser-induced phase change in GST. Depending on the differences in pulse duration, laser energy, repetition rates, and numbers of laser pulses, GST films could end up in partially crystallized intermediate states. These intermediate states exhibit multiple different optical properties (optical constants or reflectivity) and electrical properties (resistivity or conductivity), thus

* Corresponding author.
E-mail address: junyingli@zju.edu.cn (J. Li).

https://doi.org/10.1016/j.optlastec.2021.107393
Received 28 January 2021; Received in revised form 18 June 2021; Accepted 9 July 2021
Available online 3 August 2021

leading to multi-level response in phase-change-involved devices [2,4,16–20]. Therefore, controlling the PCMs to change among multiple intermediate states is so called multi-level switching [16–17,21]. Intermediate phase change states were usually simply considered as the mixing states of amorphous and crystalline phases with different ratio. However, in fact, laser-induced multi-level switching was found to result in changes of chemical bonds and electronic polarizability of GST [19].

Raman spectroscopy is a powerful tool in detecting the local vibration mode of the material, and therefore offers a powerful means for observing atomic bonding and structures of GST thin film during the multi-level switching process. Wang *et al.* [22] analyzed the evolution of micro-Raman spectra of metastable phase to identify the power threshold of phase transformation. Wei *et al.* [19] investigated the changes of chemical bonds and structural evolution of GST film induced by the different laser fluence via Raman spectra analysis. Fan *et al.* [23] indicated that the dominant characteristic peaks were sensitive to the size of nanocrystal in GST films with accumulated laser pulses irradiations. Zhou *et al.* [24] investigated the crystallization of GST thin films induced by an excimer laser, and formation of Te crystal due to high photon energy at ultraviolet wavelength was confirmed via Raman spectroscopy. It is worth pointing out that although some work has been done on Raman study of laser-induced multi-level switching, our work has systematically evidenced the evolution of the bonding state of GST phase transition intermediate states that supplements state-of-the-art.

Here, we realized multi-level switching of GST thin films using a nanosecond pulse laser with different pulse duration, energy and pulse numbers. Intermediate states generated by laser-induced multi-level switching were characterized with reflection measurement and Raman spectroscopy. The similarities and differences of laser-induced phase changes and isothermal annealed ones were first analyzed. The effect of nanosecond-laser-induced multi-level switching on $GeTe_{4-n}Ge_n$ (n = 0, 1, 2) tetrahedral components and Sb_mTe_3 (m = 1, 2) structural units in GST thin films were analyzed in detail.

2. Experiment

Amorphous GST (AM-GST) thin films with a thickness of 35 nm were deposited on Si(1 0 0) wafers via thermal evaporation with a base pressure of 1.2×10^{-4} Pa and a deposition rate of ~ 10 Å/s. To isothermally crystallize the as-deposited GST thin films, a temperature controlling stage (Instec.inc) with a temperature stability of ± 0.05 ℃ were used to anneal the AM-GST films at various temperature between 100 ℃ and 300 ℃ in nitrogen atmosphere for 30 min. The stoichiometry of GST thin films was measured via energy disperse spectroscopy (EDS) and the phases and lattice structure of GST thin films were confirmed by the X-Ray Diffraction (XRD).

Laser-induced multi-level switching of GST thin films was achieved via a customized 532 nm nanosecond pulse laser with tunable repetition rate up to 100 kHz and pulse width varying from 5 to 250 ns. The drive current of the laser varies from 0 to 10A. While driven by a certain current, the single pulse energy gradually decreases from 300(10A & 5 ns) to 0 nJ ± 3 nJ with the increase of pulse width. The laser beam was coupled into a 40 × objective lens (0.6NA), and focused on the film surface vertically with a spot diameter of about 12 μm. To guarantee the repeatability of measurements among samples, another low-power continuous-wave laser with the wavelength of 852 nm was irradiated on the GST thin film and its reflectance was monitored as reference.

The irradiation spot reflection spectra were measured by a home-built micro-area reflection system. The reflection light source was either a 532 nm CW laser or a halogen tungsten lamp. The light beam was focused on a 50 × inverted objective lens, and the focusing spot on the samples surface had a diameter of about 5 μm, which was significantly smaller than the laser-annealed area. The position of the probe light spot on the samples was observed via a CCD camera and aligned via multi-axis motorized stages. The reflection spectra of the corresponding irradiation spots were collected by a spectrometer (iHR550 HORIBA). Each measurement was repeated for 3 to 5 times.

The Raman spectra of GST films were measured using a Raman spectrometer (HORIBA, LabRAM Xplora Plus). The power of the 638-nm-wavelength excitation laser that reached the surface of GST films was kept below 3 mW to avoid laser-irradiated changes in GST during measurement, and the spot size was smaller than 1 μm. For each Raman spectrum, the measurement was repeated for 3 times, and the average spectrum was ultimately employed.

3. Results and discussion

3.1. Isothermal-annealing-induced crystallization

Before other experiments, the thermal-evaporated GST thin films were characterized. The atomic ratio of each element in the as-deposited GST films is shown in Table 1. 5 measurement points were randomly chosen on a 1.5 × 1.5 cm^2 GST film and showed a good homogeneity. The films exhibited a composition of $Ge_{22.504\pm1.164}Sb_{23.032\pm1.365}Te_{54.464\pm1.193}$ that is close to ideal stoichiometry. This guarantees that the amorphous (AM) GST films were able to crystallize into correct face-centered cubic (FCC) metastable state (when annealed at 150 ℃) and hexagonal-close-packed (HCP) equilibrium state (when annealed at 250 ℃), as shown in the XRD patterns in Fig. 1a. The optical constants of AM and FCC (150 ℃ & 30 min) films were measured and fitted using ellipsometry, as shown in Fig. 1b. The huge contrast of optical constants after the phase transition in the GST thin films ensures the multiple reflectivity of intermediate states during multi-level switching.

Subsequently, the GST thin films, which were isothermally annealed at various temperature from 100 ℃ to 300 ℃, were characterized by Raman spectroscopy, see Fig. 1c. Both the as-deposited and 100 ℃-annealed GST thin films had a large envelope peak at ~ 145 cm^{-1} which was related to Sb-Te vibrations in Sb_mTe_3 (m = 1, 2) pyramidal units [13,25–27]. Another peak at ~ 125 cm^{-1}, which resulted from the A_1 mode of $GeTe_{4-n}Ge_n$ (n = 0, 1, 2) corner-sharing tetrahedral units [13,25–28] was weaker than the above-mentioned peak at ~ 145 cm^{-1}, due to lower polarizability of GeTe bonds compared to Sb_2Te_3 component [13,28]. These two broad peaks verified the amorphous phase of GST.

With a further increase of the annealing temperature to 150 ℃ where GST crystallized into FCC phase, the Raman spectra started to show three peaks at ~ 105 cm^{-1}, ~135 cm^{-1}, and ~ 160 cm^{-1}. Among them, first two peaks evolved from the Raman peak at ~ 125 cm^{-1} in AM GST ($GeTe_{4-n}Ge_n$ vibration modes). The peak at ~ 105 cm^{-1} was attributed to softened A_1 modes of corner-sharing $GeTe_4$ tetrahedra [13,22,29], and the peak at ~ 135 cm^{-1} was ascribed to the A_1 mode of corner-sharing $GeTe_{4-n}Ge_n$ (n = 1, 2) tetrahedra [13,26]. In other words, the peak at 105 cm^{-1} could be attributed to the Te-rich units, while the peak at 135 cm^{-1} could be associated with Ge-rich units [28,30]. Meanwhile, the peak at ~ 160 cm^{-1} corresponded to the vibration of Sb_mTe_3 (m = 1, 2) subsystem (namely $SbTe_3$ pyramids or crystalline Sb_2Te_3 [13,21,30]). After that, annealing at 200 ℃ (where GST also presented FCC lattice) led to an enhancement of the Raman peak at ~ 105 cm^{-1}, similar to previously reported results [19,29].

As the annealing temperature increased to 250 ℃ and 300 ℃, the

Table 1
Atomic ratio of as-deposited GST thin films measured by EDS.

Points	Ge (at.%)	Sb (at.%)	Te (at.%)
1	21.28	22.22	56.50
2	22.73	23.42	53.85
3	24.25	21.19	54.56
4	22.65	23.58	53.77
5	21.61	24.75	53.64
Average(at.%)	22.504 ± 1.164	23.032 ± 1.365	54.464 ± 1.193

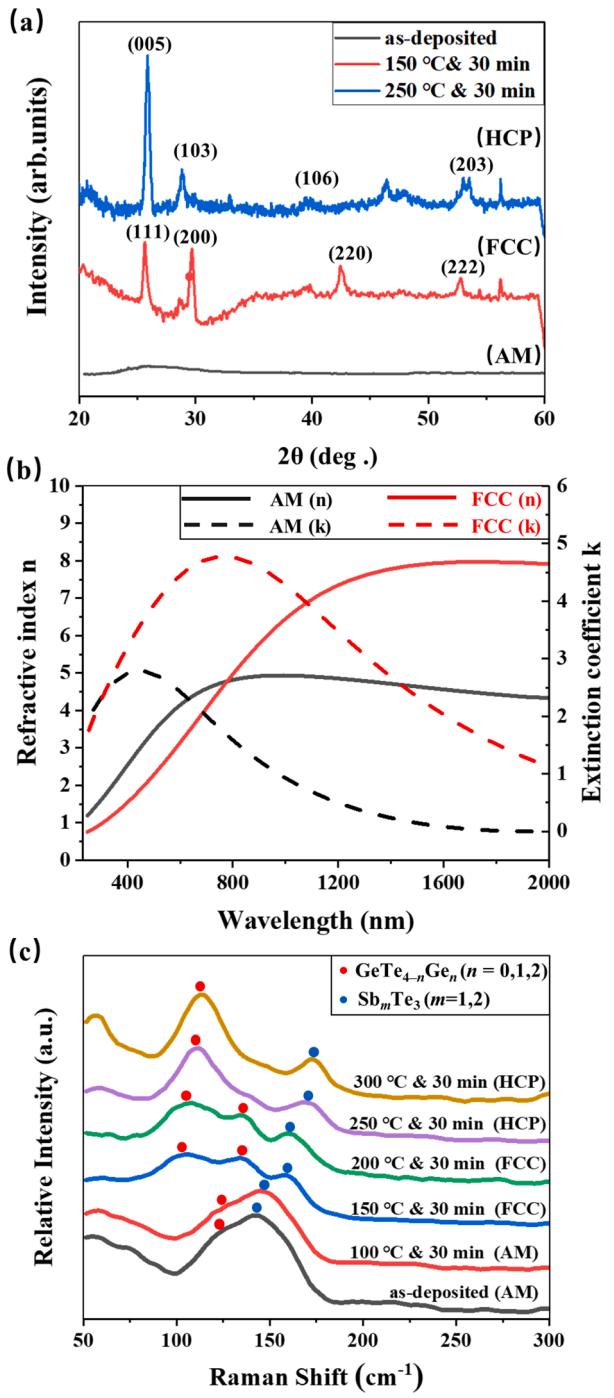

Fig. 1. (a) XRD patterns of GST films; (b) optical constants of AM and FCC GST films; (c) the Raman spectra of GST film annealed at various temperatures (the red dots marked peaks related to vibration of $GeTe_{4-n}Ge_n$ ($n = 0, 1, 2$) structural units, and the blue dots marked the peaks resulted from vibration of Sb_mTe_3 ($m = 1, 2$) structural units).

GST film transformed into the HCP phase. The vibration of $GeTe_{4-n}Ge_n$ tetrahedra and $A_{1g}(2)$ modes of hexagonal Sb_2Te_3 led to Raman peaks at $\sim 112\ cm^{-1}$ and $\sim 170\ cm^{-1}$, respectively [13,26,31].

Hence, in a thermally crystallized GST, both $GeTe_{4-n}Ge_n$ ($n = 0, 1, 2$) subsystem (marked with red dot in Fig. 1c) and Sb_mTe_3 ($m = 1, 2$) subsystem (marked with blue dot) of GST alloys contributed to the phase transition under isothermal conditions. Also, for a certain lattice structure, higher annealing temperature led to stronger Raman peak in lower frequency.

3.2. Laser-induced multi-level switching

In this section, both as-deposited and thermally crystallized GST thin films were employed to demonstrate laser-induced multi-level switching. The effect of pulse number, pulse width and pulse energy on intermediate states was investigated.

3.2.1. Multi-level switching with varying pulse number

Fig. 2a shows an optical image of phase change dots on an AM-GST background film induced by nanosecond laser pulses with the pulse width varying from 5 to 60 ns and the pulse number varying from 1 to 16 (drive current fixed at 8A). When switching via multiple pulses, the interval between two pulses was set to 1 ms to ensure the material was thermally relaxed. Thus, the crystallization level of the GST film depends only on the total number of incident pulses. Overall, laser fluence was varied from 20.9 to 78.8 mJ/cm^2 (8A & 60 ns ~ 8A & 5 ns). As shown in the optical image, the size and brightness of the irradiation dots gradually increases with the increase of the exposure dose (i.e. more pulse number and/or higher fluence of the laser).

In order to more effectively illustrate the effect of multi-level switching, the normalized reflectivity of irradiation dots induced by varying numbers of laser pulses was shown in Fig. 2b. With increasing pulse number, the reflectivity gradually increases, due to the increasing refractive index of GST. This is a typical phenomenon of multi-level switching. Note that the error bars were about ± 10%, which resulted from the alignment errors between the irradiation dots and the focused spot.

Due to the Gaussian energy distribution of the laser beam, toroidal shell could be observed in the irradiation area with relatively short pulse width (high energy). Fig. 2d shows the optical images of three typical phase change dots (corresponding to A ~ C respectively marked in Fig. 2a). In these irradiated marks, ablated region, melt-quenched-amorphous (M−amorphous) region, and crystallized region on AM-GST background film could be distinguished from Raman spectra in the bottom panel. The ablated region was darker under optical microscope due to comparatively lower reflectivity of Si than that of GST film. And in M−amorphous region, evidenced by a remarkable broad peak at $\sim 145\ cm^{-1}$ with a weak shoulder at $\sim 125\ cm^{-1}$ on Raman spectra, the film was melted and then rapidly quenched into AM state due to short pulse width. With regards to the laser-induced crystallized region, Raman peaks at $\sim 105\ cm^{-1}$ and $\sim 135\ cm^{-1}$ were both observed, but the peak at $\sim 160\ cm^{-1}$ in the Raman spectra of thermally annealed GST films was very weak here.

More than 8 pulses with a pulse fluence higher than $\sim 78.8\ mJ/cm^2$ could lead to ablation of GST at the center of the spot (marked by the black arrow in region A of Fig. 2d), followed by a M−amorphous annulus (marked by the red arrow) and a crystallized one (marked by the blue arrow). This kind of irradiated dots were categorized as ablated marks. With longer pulse width (lower fluence) of the laser, the center of irradiated dots became M−amorphous (namely M−amorphous mark), and a crystallized annulus encircled it on the AM-GST background (shown in region B). A further decrease of laser fluence to 50.9 mJ/cm^2 (pulse widths larger than 20 ns) led to crystallized marks (typically shown in region C). Finally, as the laser fluence decreased below ~ 20.9 mJ/cm^2, the crystallized dots almost disappeared.

It is very interesting to notice that among the multi-level switching, the intensity of different Raman peaks was changing. Fig. 2c shows the Raman spectra of crystallization dots induced by varying numbers of laser pulses with the pulse width fixed at 30 ns. With the increase of pulse number, the intensity of Raman peak at ~105 cm^{-1} gradually increased and the intensity at ~135 cm^{-1} decreased. That means more pump pulses may lead to the forming of more Te-rich tetrahedral components in $GeTe_{4-n}Ge_n$ structural units of GST films.

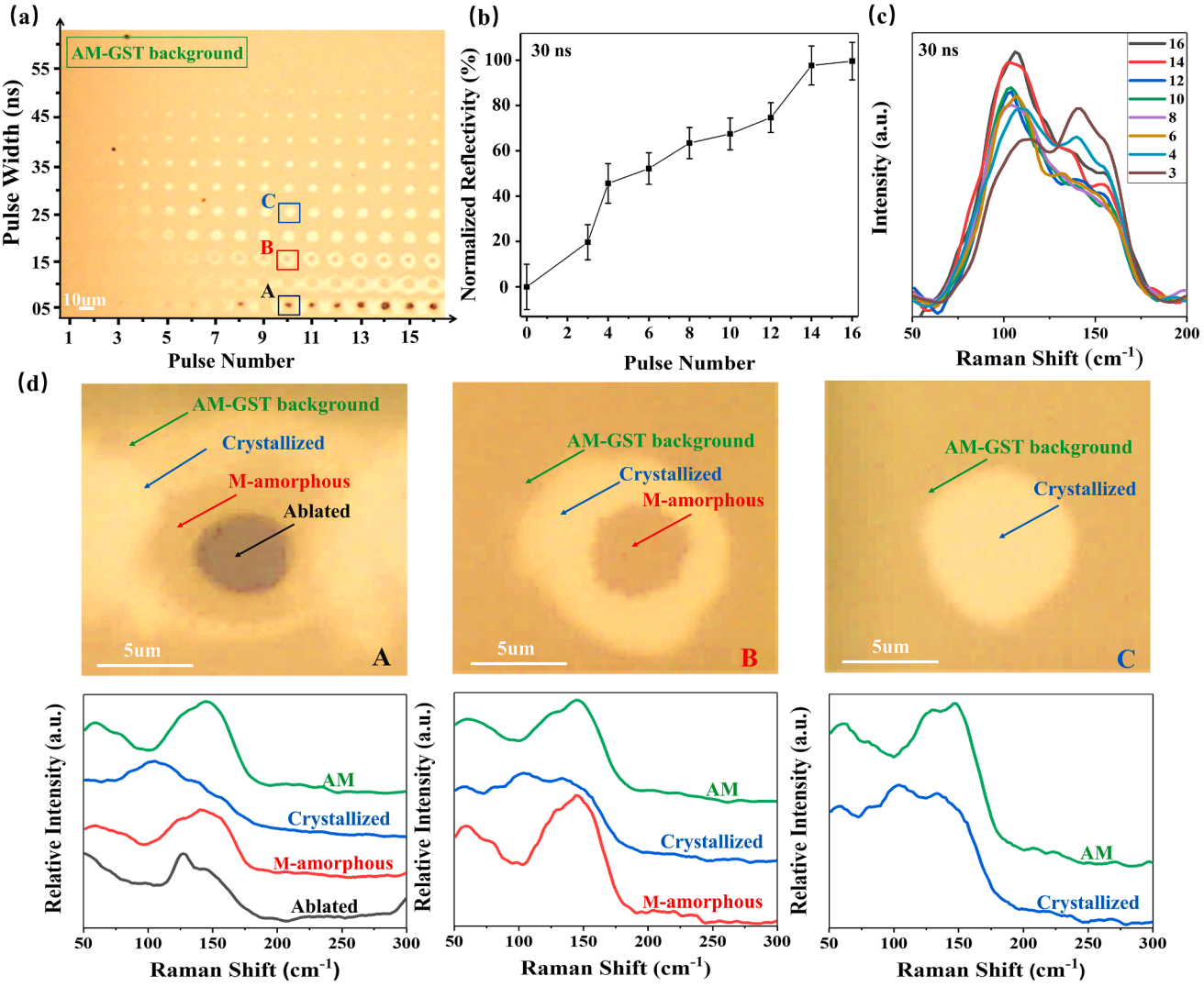

Fig. 2. (a) The irradiation marks on an AM-GST background film induced by nanosecond laser pulses with different pulse numbers and pulse widths; (b) normalized reflectivity of the irradiation marks induced by laser pulses with a pulse width of 30 ns and varying pulse numbers; (c) Raman spectra at the center of the irradiation marks induced by laser pulses with the pulse width of 30 ns and varying pulse numbers; (d) the enlarged one from A to C irradiation marks in Fig. 2a, with corresponding Raman spectra in bottom panel.

3.2.2. Evolution of Raman peaks ascribed to $GeTe_{4-n}Ge_n$ tetrahedra in laser-induced multi-level switching

In order to know if there is any other parameter of laser other than pulse number that also have influences on the formation of the above-mentioned Te-rich component, pulse number of the nanosecond laser was fixed to 10 with a repetition rate of 100 kHz in the following experiment. Fig. 3a shows an optical image of irradiation dots on AM-GST background film with the pulse widths varied from 5 to 70 ns as the drive current increases from 7.6 to 8.8A. Correspondingly, laser fluence approximately varied from 10.8 to 90.6 mJ/cm^2 (7.6A & 65 ns ~ 8.8A & 5 ns). Similarly, the irradiation dots also exhibited ablated, M−amorphous and crystallized areas. Although the ablated region of GST thin film itself is hard to analyze due to the laser damage, the material evaporation was evidenced by the Si peak of the Raman spectrum (see Fig. 3b). Severer ablation leads to more GST evaporation and stronger Si(1 0 0) peak at ~ 520 cm^{-1} in Raman spectra, which helped semi-quantitatively characterize the degree of laser damage to the film.

Similarly, to confirm the realization of multi-level switching, reflection spectra of the irradiation spots (in the purple dotted box in Fig. 3a) that crystallized by laser pulses with different laser fluence were measured. The normalized reflectivity at 532 nm wavelength were extracted and plotted in Fig. 4a, manifesting a typical multi-level switching process. The measurements were repeated for 3 times and the standard deviation was within ± 6%.

In Fig. 4b, Raman spectra of crystallized dots (marked with the purple box in Fig. 3a) induced by laser pulses with a drive current of 8A and a pulse width varying from 20 to 55 ns was shown. Note that for a certain pulse number, the enhancement of Raman peak at ~105 cm^{-1} with the increase of pulse energy for laser-crystallized GST film was also observed. The typical Raman peaks of laser-crystallized GST at ~105 cm^{-1} and ~ 135 cm^{-1} resulted from $GeTe_{4-n}Ge_n$ ($n = 0, 1, 2$) tetrahedra were illustrated by the blue triangles. Dominant peaks that were enhanced by high energy laser pulses were marked with dark-color triangles and relatively weaker peaks marked with light ones. Apparently, for laser pulses with a fluence of 26.4 mJ/cm^2 (@ 50 ns pulse width) and lower, there was no obvious difference between the intensity of Raman peaks at ~105 cm^{-1} and ~ 135 cm^{-1}. However, increasing the laser fluence before reaching the amorphization state (fluence of 50.9 mJ/cm^2 @ 20 ns pulse width) resulted in the dominant peak at ~ 105 cm^{-1} with a weaker one at ~ 135 cm^{-1}. This indicated that more Te-rich tetrahedra in $GeTe_{4-n}Ge_n$ ($n = 0, 1, 2$) units tend to form when GST was crystallized by laser pulses with higher energy.

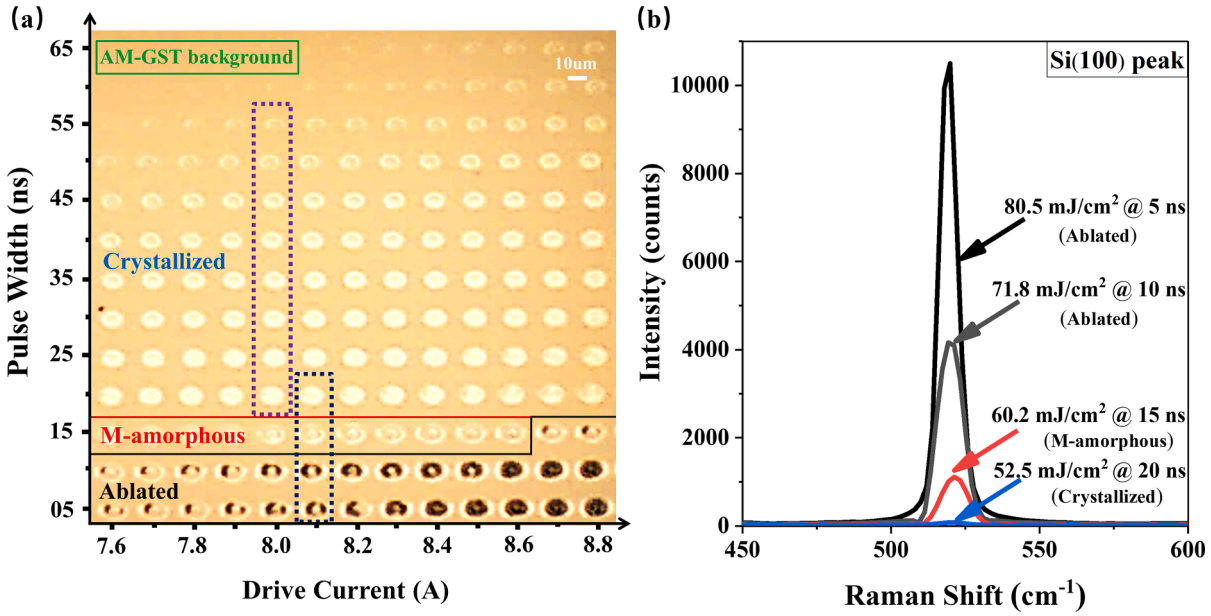

Fig. 3. (a) The irradiation marks on an AM-GST film induced by 10 laser pulses with varying drive current and pulse widths; (b) the variation tendency of Si(1 0 0) peak in irradiation marks with black dotted line region in Fig. 3a.

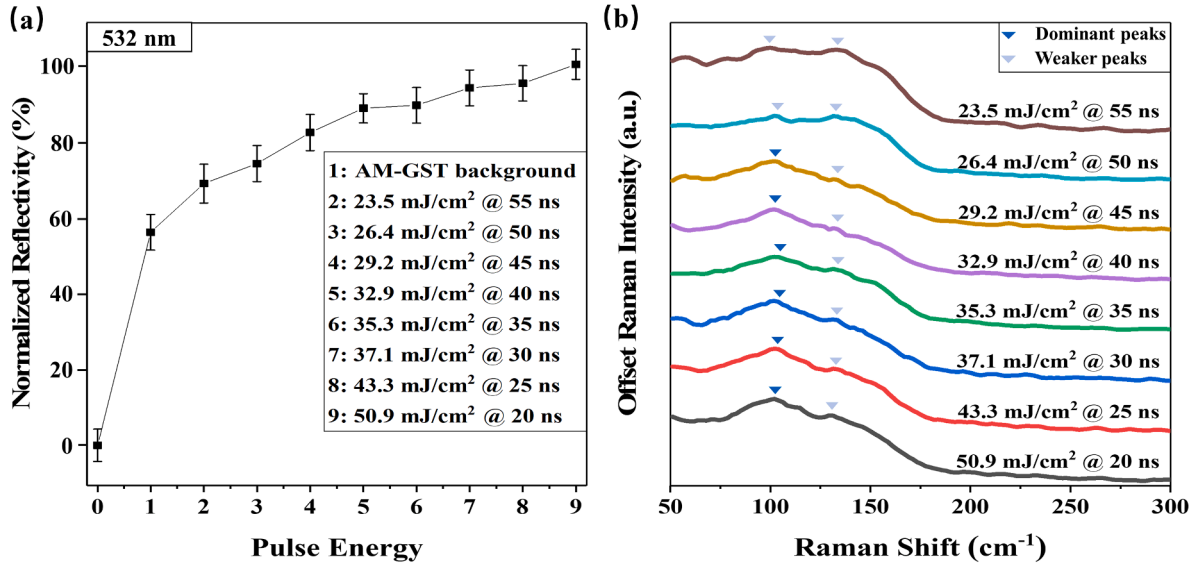

Fig. 4. (a) The increase of the normalized reflectivity of corresponding irradiation dots with the increase of nanosecond laser energy; (b) the enhancement of Raman peak of Te-rich components in $GeTe_{4-n}Ge_n$ units of crystallized GST at ~ 105 cm^{-1} with the increase of fluence of the laser.

To clearly present the role that $GeTe_{4-n}Ge_n$ (n = 0, 1, 2) tetrahedra plays in the laser-induced multi-level switching of GST, Fig. 5 comparatively shows typical Raman spectra of cubic-phase GST resulted from isothermal annealing and laser irradiation. Obviously, as illustrated by the vertical dash line in Fig. 5, the Raman peak at ~ 160 cm^{-1} for isothermal annealed GST was absent from the spectra of laser-crystallized one. In other words, the $GeTe_{4-n}Ge_n$ (n = 0, 1, 2) component of GST alloys is mainly responsible for the laser-induced phase transition [22,32]. It is more interesting to further investigate why more Te-rich tetrahedral components formed than Ge-rich components did in $GeTe_{4-n}Ge_n$ subsystem for higher-level of laser-induced multi-level crystallization (indicated by increase of the intensity of Raman peak at ~105 cm^{-1} over the peak at ~135 cm^{-1}). Fig. 5 shows that the enhancement of the intensity of the Raman peak at ~105 cm^{-1} is found in both higher-temperature isothermal annealing and higher-energy laser irradiation (marked with dark blue triangles). This manifests that the forming of Te-rich tetrahedra may originate from the heating effect of the incident laser, and more Te-rich tetrahedra in $GeTe_{4-n}Ge_n$ units form as the crystallinity of GST increases.

3.2.3. *The suppression of the Raman peak related to Sb_mTe_3 subsystem*

As mentioned above, the as-deposited GST crystallized by nanosecond laser pulses shows a very weak Raman peak of Sb_mTe_3 (m = 1, 2) subsystem compared with the one crystallized by isothermal annealing. It reasonably rises a question that whether it would be the same situation when an FCC phase GST film (resulted from isothermal annealing) is further crystallized by nanosecond laser pulses. Therefore, to further verify the influence of nanosecond laser, an as-deposited GST thin film was first isothermally annealed at 200 °C for 30 min in N_2 atmosphere, and then switched by nanosecond laser pulses with different energy to

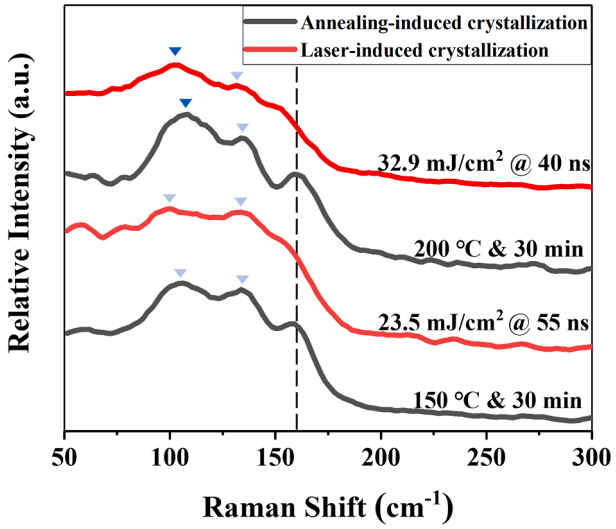

Fig. 5. Comparison of Raman spectra of crystallized GST resulted from isothermal annealing and laser irradiation (dominant peaks marked with dark-color triangles and weaker peaks marked with light ones).

write a dot array, as shown in Fig. 6a. 10 pulses with a repetition rate of 100 kHz was employed for each dot. Pulse widths of laser varied from 15 to 27 ns and the drive current increased from 6.5 to 8A, which led to laser fluence between approximately 22.5 and 58.6 mJ/cm^2 (6.5A & 27 ns ~ 8A &15 ns). The isothermally annealed GST film could also be amorphized or crystallized again by laser pulses (confirmed by Raman spectra, typically as shown in Fig. 6b). The switching energy threshold was obviously lower due to higher absorption of crystallized GST thin film than AM-GST.

Dot D in Fig. 6a is a typical laser-crystallized mark on isothermally annealed GST background. A comparison between the Raman spectra of dot D and isothermally annealed FCC-GST background are shown in the Fig. 6b. Note that the Raman peak of isothermally annealed GST at ~ 160 cm^{-1} is also weakened after crystallized once more by nanosecond laser pulses (marked by the dash line). This confirms that the $GeTe_{4-n}Ge_n$ subsystem largely contributes to phase transition in GST resulted from laser irradiation no matter what state GST was at before laser exposure, while the effect of Sb_mTe_3 subsystem may be suppressed to some extent.

Another interesting finding is the blue shift (shown in blue arrow) of Raman peaks at ~ 105 cm^{-1} and ~ 135 cm^{-1} after the isothermally annealed GST is laser crystallized again. This shift is considered to be related to the changes in the bond length [33] of GST film caused by the stress due to rapid local temperature changes in the film. Typically, isothermal annealing that maintains a steady environment and atomic structures of the whole film can be re-arranged in a long-enough time duration. However, for laser-induced switching, steep heating profile is generated within a local area on the film. Laser beam with a Gaussian distribution even intensifies the non-uniform local heating, and the thickness of the film in this area is abruptly changed in a very short pulse duration. Hence, the thickness difference between laser-irradiated area and background may lead to tensile stress. This may result in longer Ge-Te bond in $GeTe_{4-n}Ge_n$ units in laser-induced crystallized area compared to the annealed GST background, thus leading to a blue shift of Raman peaks.

4. Conclusions

In summary, we achieved multi-level switching in GST thin films induced by a 532 nm nanosecond pulse laser with different pulse duration, energy and pulse numbers. The changes of bonds and structural features resulted from laser irradiation were compared with the isothermal annealing one by Raman spectroscopy. It is found that the Raman peak ascribed to Sb_mTe_3 subsystem is suppressed by laser pulses. Meanwhile, $GeTe_{4-n}Ge_n$ (n = 0, 1, 2) tetrahedra plays a decisive role in laser-induced crystallization of both as-deposited and annealed-crystallized GST background thin films. Laser pulses with higher energy or more shots lead to the forming of more Te-rich tetrahedral components rather than Ge-rich ones in $GeTe_{4-n}Ge_n$ subsystem of GST film for higher-level laser-induced crystallization. This is attributed to the heating effect of laser pulses on GST thin films, since similar trend is also observed for GST films annealed at higher temperature. This may be associated with distortion, stress and vacancy ordering resulted from locally and partially crystallization in laser-induced multi-level switching, which can be further studied with in-situ HRTEM imaging. Our findings provide a possible structure evolution to GST phase change dynamics.

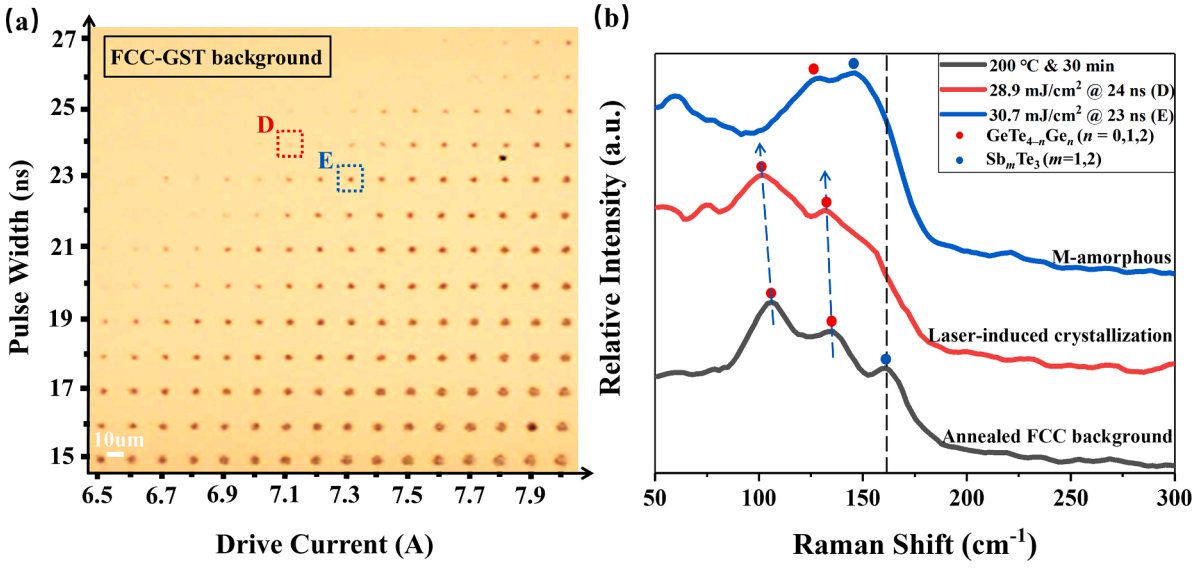

Fig. 6. (a) Irradiation marks induced by laser pulses (with different drive current and pulse widths) on an isothermally annealed cubic phase GST film; (b) comparison of Raman spectra of crystallized and M−amorphous GST resulted from isothermal annealing and laser irradiation (the peaks showed with the red dots ascribed to vibration of $GeTe_{4-n}Ge_n$ (n = 0, 1, 2) structural units, and the peaks marked by the blue dots resulted from vibration of Sb_mTe_3 (m = 1, 2) structural units).

CRediT authorship contribution statement

Jia Du: Conceptualization, Methodology, Software, Investigation, Writing – original draft. **Zhangjian Mu:** Validation, Formal analysis, Visualization, Software. **Lan Li:** Resources, Writing - review & editing, Supervision. **Junying Li:** Resources, Writing - review & editing, Supervision.

Declaration of Competing Interest

The authors declare that they have no known competing financial interests or personal relationships that could have appeared to influence the work reported in this paper.

Acknowledgments

This work was supported by National Key Research and Development Program of China (No. 2019YFB2203003), Shanghai Sailing Program (No. 19YF1435400), the Open Fund of the State Key Laboratory of Integrated Optoelectronics (No. IOSKL2020KF05), and the Fundamental Research Funds for the Central Universities (No. 2021QNA5007 and No. 2020XZZX005-07). We would like to thank Yaoguang Ma and Xinhang Liu for assistance with measurements on reflectivity.

References

[1] T. Alexoudi, G.T. Kanellos, N. Pleros, Optical RAM and integrated optical memories: a survey, Light Sci. Appl. 9 (1) (2020), https://doi.org/10.1038/s41377-020-0325-9.
[2] J. Feldmann, M. Stegmaier, N. Gruhler, C. Ríos, H. Bhaskaran, C.D. Wright, W.H. P. Pernice, Calculating with light using a chip-scale all-optical abacus, Nature, Communications. 8 (1) (2017), https://doi.org/10.1038/s41467-017-01506-3.
[3] M.H.R. Lankhorst, B.W.S.M.M. Ketelaars, R.A.M. Wolters, Low-cost and nanoscale non-volatile memory concept for future silicon chips, Nat. Mater. 4 (4) (2005) 347–352.
[4] M. Wuttig, H. Bhaskaran, T. Taubner, Phase-change materials for non-volatile photonic applications, Nat. Photonics 11 (8) (2017) 465–476.
[5] W. Zhang, R. Mazzarello, M. Wuttig, E. Ma, Designing crystallization in phase-change materials for universal memory and neuro-inspired computing, Nat. Rev. Mater. 4 (3) (2019) 150–168.
[6] B. Gholipour, J. Zhang, K.F. MacDonald, D.W. Hewak, N.I. Zheludev, An All-Optical, Non-volatile, Bidirectional, Phase-Change Meta-Switch, Adv. Mater. 25 (22) (2013) 3050–3054.
[7] Q. Zhang, Y. Zhang, J. Li, R. Soref, T. Gu, J. Hu, Broadband nonvolatile photonic switching based on optical phase change materials: beyond the classical figure-of-merit, Opt. Lett. 43 (1) (2018) 94, https://doi.org/10.1364/OL.43.000094.
[8] C.R. de Galarreta, A.M. Alexeev, Y.-Y. Au, M. Lopez-Garcia, M. Klemm, M. Cryan, J. Bertolotti, C.D. Wright, Nonvolatile Reconfigurable Phase-Change Metadevices for Beam Steering in the Near Infrared, Adv. Funct. Mater. 28 (10) (2018) 1704993, https://doi.org/10.1002/adfm.v28.1010.1002/adfm.201704993.
[9] P. Hosseini, C.D. Wright, H. Bhaskaran, An optoelectronic framework enabled by low-dimensional phase-change films, Nature 511 (7508) (2014) 206–211.
[10] J. Hu, V. Tarasov, A. Agarwal, L. Kimerling, N. Carlie, L. Petit, K. Richardson, Fabrication and testing of planar chalcogenide waveguide integrated microfluidic sensor, Opt. Express 15 (5) (2007) 2307, https://doi.org/10.1364/OE.15.002307.
[11] M. Bouska, S. Pechev, Q. Simon, R. Boidin, V. Nazabal, J. Gutwirth, E. Baudet, P. Nemec, Pulsed laser deposited GeTe-rich GeTe-Sb_2Te_3 thin films, Sci. Rep 6 (2016) 26552.
[12] S. Buller, C. Koch, W. Bensch, P. Zalden, R. Sittner, S. Kremers, M. Wuttig, U. Schürmann, L. Kienle, T. Leichtweiß, J. Janek, B. Schönborn, Influence of Partial Substitution of Te by Se and Ge by Sn on the Properties of the Blu-ray Phase-Change Material $Ge_8Sb_2Te_{11}$, Chem. Mater 24 (18) (2012) 3582–3590.
[13] P. Němec, V. Nazabal, A. Moreac, J. Gutwirth, L. Beneš, M. Frumar, Amorphous and crystallized Ge–Sb–Te thin films deposited by pulsed laser: Local structure using Raman scattering spectroscopy, Mater. Chem. Phys. 136 (2–3) (2012) 935–941.
[14] D. Loke, T.H. Lee, W.J. Wang, L.P. Shi, R. Zhao, Y.C. Yeo, T.C. Chong, S.R. Elliott, Breaking the Speed Limits of Phase-Change Memory, Science 336 (6088) (2012) 1566–1569.
[15] V. Weidenhof, I. Friedrich, S. Ziegler, M. Wuttig, Laser induced crystallization of amorphous $Ge_2Sb_2Te_5$ films, J. Appl. Phys. 89 (6) (2001) 3168–3176.
[16] Q. Wang, J. Maddock, E.T.F. Rogers, T. Roy, C. Craig, K.F. Macdonald, D. W. Hewak, N.I. Zheludev, 1.7 Gbit/in.2 gray-scale continuous-phase-change femtosecond image storage, Appl. Phys. Lett. 104 (12) (2014) 121105, https://doi.org/10.1063/1.4869575.
[17] F. Yang, L. Xu, J. Chen, J. Xu, Y. Yu, Z. Ma, K. Chen, Nanoscale multilevel switching in $Ge_2Sb_2Te_5$ thin film with conductive atomic force microscopy, Nanotechnology 27 (3) (2016) 035706, https://doi.org/10.1088/0957-4484/27/3/035706.
[18] X. Sun, A. Lotnyk, M. Ehrhardt, J.W. Gerlach, B. Rauschenbach, Realization of Multilevel States in Phase-Change Thin Films by Fast Laser Pulse Irradiation, Adv. Opt. Mater. 5 (12) (2017).
[19] T. Wei, J. Wei, K. Zhang, H. Zhao, L. Zhang, Grayscale image recording on $Ge_2Sb_2Te_5$ thin films through laser-induced structural evolution, Sci. Rep. 7 (1) (2017), https://doi.org/10.1038/srep42712.
[20] X. Sun, M. Ehrhardt, A. Lotnyk, P. Lorenz, E. Thelander, J.W. Gerlach, T. Smausz, U. Decker, B. Rauschenbach, Crystallization of $Ge_2Sb_2Te_5$ thin films by nano- and femtosecond single laser pulse irradiation, Sci. Rep. 6 (1) (2016), https://doi.org/10.1038/srep28246.
[21] S. Wen, Y. Meng, M. Jiang, Y. Wang, Multi-level coding-recoding by ultrafast phase transition on $Ge_2Sb_2Te_5$ thin films, Sci. Rep. 8 (1) (2018), https://doi.org/10.1038/s41598-018-23360-z.
[22] G. Wang, C. Li, D. Shi, Y. Zhang, X. Shen, Laser-induced metastable phase in crystalline phase-change films by confocal Raman spectrometer, Spectrochim. Acta. A. Mol. Biomol. Spectrosc. 205 (2018) 551–556.
[23] T. Fan, F.R. Liu, W.Q. Li, J.C. Guo, Y.H. Wang, N.X. Sun, F. Liu, Study on accumulated crystallization characteristics of amorphous $Ge_2Sb_2Te_5$ induced by multi-pulsed laser irradiations with different fluences, Semicond. Sci. Technol. 33 (7) (2018) 075009, https://doi.org/10.1088/1361-6641/aac370.
[24] W.P. Zhou, F.R. Liu, N. Bai, Y.H. Wan, X. Lin, J.M. Chen, Crystallization of amorphous $Ge_2Sb_2Te_5$ films induced by an ultraviolet laser, Appl Surf Sci 285 (2013) 97–101.
[25] S. Kozyukhin, Y. Vorobyov, A. Sherchenkov, A. Babich, N. Vishnyakov, O. Boytsova, Isothermal crystallization of $Ge_2Sb_2Te_5$ amorphous thin films and estimation of information reliability of PCM cells, physica. status. solidi (a) 213 (7) (2016) 1831–1838.
[26] Z. Xu, C. Chen, Z. Wang, K. Wu, H. Chong, H. Ye, Optical constants acquisition and phase change properties of thin films based on spectroscopy, RSC Adv. 8 (37) (2018) 21040–21046.
[27] S. Kozyukhin, P. Lazarenko, Y. Vorobyov, A. Baranchikov, V. Glukhenkaya, M. Smayev, A. Sherchenkov, Y. Sybina, A. Polohin, V. Sigaev, Laser-induced modification and formation of periodic surface structures (ripples) of amorphous GST225 phase change materials, Opt. Laser Technol. 113 (2019) 87–94.
[28] K.S. Andrikopoulos, S.N. Yannopoulos, A.V. Kolobov, P. Fons, J. Tominaga, Raman scattering study of GeTe and $Ge_2Sb_2Te_5$ phase-change materials, J. Phys. Chem. Solids. 68 (5-6) (2007) 1074–1078.
[29] P. Němec, A. Moreac, V. Nazabal, M. Pavlišta, J. Přikryl, M. Frumar, Ge–Sb–Te thin films deposited by pulsed laser: An ellipsometry and Raman scattering spectroscopy study, J. Appl. Phys. 106 (10) (2009) 103509, https://doi.org/10.1063/1.3259435.
[30] Z. Zhu, F.R. Liu, Z.M. Wang, Z.K. Fan, F. Liu, N.X. Sun, Comparative study on crystallization characteristics of amorphous $Ge_2Sb_2Te_5$ films by an ultraviolet laser radiation and isothermal annealing, Appl. Surf. Sci. 335 (2015) 184–188.
[31] G.C. Sosso, S. Caravati, C. Gatti, S. Assoni, M. Bernasconi, Vibrational properties of hexagonal Ge(2)Sb(2)Te(5) from first principles, J. Phys. Condens. Matter. 21 (24) (2009) 245401, https://doi.org/10.1088/0953-8984/21/24/245401.
[32] A.V. Kolobov, P. Fons, J. Tominaga, Phase-change optical recording: Past, present, future, Thin Solid Films 515 (19) (2007) 7534–7537.
[33] Y. Yan, X.u. Zhou, H. Jin, C.-Z. Li, X. Ke, G. Van Tendeloo, K. Liu, D. Yu, M. Dressel, Z.-M. Liao, Surface-Facet-Dependent Phonon Deformation Potential in Individual Strained Topological Insulator Bi_2Se_3 Nanoribbons, ACS Nano 9 (10) (2015) 10244–10251.